Article Type:	Invited Methods Article - JoVE Produced Video
Manuscript Number:	JoVE61115R2
Full Title:	Brillouin Optical Time-Domain Analyzers based on Gain Spectrum Engineering
Section/Category:	JoVE Engineering
Keywords:	Distributed fiber sensing, stimulated Brillouin scattering, Brillouin optical time-domain analyzer, gain spectrum engineering, noise, measurand resolution
Corresponding Author:	Cheng Feng Technische Universität Braunschweig Braunschweig, Niedersachsen GERMANY
Corresponding Author's Institution:	Technische Universität Braunschweig
Corresponding Author E-Mail:	cheng.feng@ihf.tu-bs.de
Order of Authors:	Cheng Feng
	Thomas Schneider
Additional Information:	
Question	**Response**
Please indicate whether this article will be Standard Access or Open Access.	Standard Access (US$2,400)
Please indicate the **city, state/province, and country** where this article will be **filmed**. Please do not use abbreviations.	Braunschweig, Niedersachsen (Lower Saxony), Germany

Manuscript
Click here to
access/download;Manuscript;61115_R0_022520.docx

1 **TITLE:**

2 **Optimizing Brillouin Optical Time-Domain Analyzers Based on Gain Spectrum Engineering**

3

4 **AUTHORS AND AFFILIATIONS:**

5 Cheng Feng, Thomas Schneider

6

7 THz-Photonics Group, Technische Universität Braunschweig, Braunschweig, Germany

8

9 **Corresponding Author:**

10 Cheng Feng   (cheng.feng@ihf.tu-bs.de)

11

12 **Email of Co-author:**

13 Thomas Schneider   (thomas.schneider@tu-bs.de)

14

18

19 **SUMMARY:**

20 A protocol for Brillouin optical time-domain analyzers based on gain spectrum engineering is

21 presented. Enhancements in the sensing performance, including sensing range and measurand

22 resolution are achieved and the excess Brillouin intensity noise is studied. The protocol

23 introduces a new way to enhance distributed Brillouin sensing performance.

24

25 **ABSTRACT:**

26 Demonstrated is a unique method for sensing performance enhancement in Brillouin optical

27 time-domain analyzers (BOTDA). A Brillouin gain spectrum (BGS) is superimposed with two

28 symmetric Brillouin loss spectra (BLS). This leads to a complex engineered spectrum shape that

29 is more resistant to the sensing system noise. Instead of only one pump and probe interaction as

30 in the conventional BOTDA setup, three optical probe waves are exploited, with one probe

31 located in the BGS and the other two symmetrically in the BLS. Due to the resistance and

32 insensitivity of the engineered spectrum shape to the noise, the sensing performance is

33 enhanced by 60% and the measurand resolution is doubled.

34

35 **INTRODUCTION:**

36 Distributed fiber sensing (DFS) is a unique mechanism that employs a whole fiber as a sensing

37 medium. It has attracted a lot of interest due to the low fiber loss; small size; and the ability to

38 be easily embedded in various structures, such as dams, bridges, and buildings, to perform

39 environment surveillance as an artificial nerve system. In comparison to applying numerous

40 traditional point sensors, such as fiber Bragg gratings (FBG), it provides a more efficient and cost-

41 effective solution in a wide range of large-scale sensing tasks, such as infrastructure and

42 structural health monitoring[1].

43

44 Current distributed sensors exploit different scattering mechanisms inside the fiber to measure

45   temperature and strain distribution. Among them, DFS based on Brillouin scattering is the most
46   attractive due to the striking advantages of the stimulated Brillouin scattering (SBS), such as high
47   signal-to-noise ratio (SNR), low threshold, and the sensitivity to both temperature[2] and strain[3].
48   SBS can be classically described as an interaction between the incident optical continuous waves
49   (CW) from the pump and the counter-propagating CW probe wave via an acoustic wave.
50   According to the conservation of energy and momentum, the probe wave is frequency
51   downshifted to the pump. This shift is called Brillouin frequency shift (BFS). Considering the finite
52   lifetime of a 10 ns acoustic wave, there is a finite spectral distribution of the refracted wave, also
53   called Brillouin gain spectrum (BGS), in which the BFS is the frequency difference between the
54   pump wave and the peak center frequency. The interaction between the waves leads to a
55   frequency down-shifted gain region and a frequency up-shifted loss region where the probe wave
56   gets amplified and attenuated, respectively. For a standard single mode fiber (SSMF) in C-Band,
57   the BFS is approximately 11 GHz and the BGS has a Lorentzian shape with an ultra-narrow full-
58   width at half maximum (FWHM) of 10–30 MHz, which can be further reduced to 3.4 MHz with
59   specific techniques[4–7]. Based on these characteristics, SBS can also be applied in microwave
60   photonics filters[8–10], optical filters[11], slow and fast light[12–14], and high resolution optical
61   spectroscopy[7,15].
62
63   One of the most promising SBS applications is distributed Brillouin sensing. These sensors exploit
64   the BFS dependence on temperature and strain. The first to be demonstrated was the Brillouin
65   optical time-domain analyzer (BOTDA)[16], which is the most consolidated time-domain distributed
66   Brillouin sensing technique. It differs from the conventional CW-SBS interaction in that it exploits
67   the SBS interaction between a pulsed pump wave and a probe CW so that the environmental
68   information is locally interrogated on every fiber section. The pump or probe frequency is usually
69   fixed while the probe or the pump frequency is scanned in the vicinity of the BFS. The probe
70   power is recorded for BGS reconstruction and the BFS is ideally the peak frequency of the local
71   BGS at each fiber section. However, due to the inevitable system noise, the BGS peak is usually
72   ambiguous and a fitting algorithm has to be applied[17], which leads to a certain estimation error
73   in frequency[18] and influences the measurand resolution.
74
75   Statistically, the BFS estimation error is inversely proportional to the system SNR. The most
76   straightforward way to enhance the SNR is to increase the pump and probe power. However,
77   these are limited by modulation instability (MI)[19] and non-local effects (NLE)[20,21] to ~20 dBm and
78   -14 dBm, respectively. Numerous techniques, such as coding[22] and Raman based inline-
79   amplification[23] have been proposed to break these limits. Recently, it has been reported that this
80   frequency error can be minimized by choosing a properly fitting algorithm[24]. Relatedly,
81   measurements exploiting the Brillouin phase and a linear fitting algorithm are also reported to
82   have a reduced frequency error[25], which indicates the potential of a well-engineered BGS to
83   sensing performance enhancement. Another option to enhance SNR is noise reduction. However,
84   according to the traditional point of view, the sensing system noise comes mainly from the
85   detector (i.e., common-mode noise, including dark noise, shot noise, etc.)[26,27] and improvement
86   is less likely.
87
88   The basic idea of this paper is to engineer the BGS by the superposition of a conventional BGS

89 with two symmetric Brillouin loss spectra (BLS) (see **Figure 1**). In comparison to a conventional
90 BGS spectrum, which follows a Lorentzian shape, the engineered spectrum is sharper and more
91 robust with the same level of system noise. Thus, the noise has less influence on the
92 determination of the peak frequency. This can be verified by collecting and fitting the BGS
93 measurement data a statistically significant number of times. Because of this better resistance to
94 the noise, sensing performance enhancements are achieved, including the sensing range by 60%
95 and doubled measurand resolution by a 50% reduced frequency error. Due to the involvement
96 of the measurement with Brillouin loss interaction in part of the engineered BGS, a direct
97 comparison of the trace noise with and without Brillouin interaction is made. Owing to the
98 circumvention of the excess Brillouin noise, the trace with the engineered BGS is much clearer.

99

100 [Place **Figure 1** here]

101

102 **PROTOCOL:**
103 **1. Selecting optimized parameters for the spectrum engineering via simulation**

104

105 1.1. Model the engineered BGS $g_{SBS}(v,z)$ with the equations[28,29]

106

107
$$G(v) = \frac{1}{2}g_0 P_p \left\{ \frac{1}{1-2j\frac{v-v_B}{\Delta v_B}} - \frac{m}{1-2j(\frac{v-v_B}{\Delta v_B}+d)} - \frac{m}{1-2j(\frac{v-v_B}{\Delta v_B}-d)} \right\} \qquad (1)$$

108

109
$$g(v,z) = \exp[G(v)L_{eff}] \cdot \exp[-2\alpha z] = g_{SBS}(v,z) \cdot \exp[j\varphi_{SBS}(v,z)] \quad (2)$$

110

111 as implemented by, for example, the supplemental MATLAB script.

112

113 NOTE: Here, $G(v)$ is the complex gain coefficient, calculated in the script as *G_complex* within the
114 *SBS_g* function for the conventional BGS or *SBS_gl* function for the engineered BGS; $g(v,z)$ is the
115 local complex Brillouin gain; and g_{SBS} and φ_{SBS} are the real and imaginary part of $g(v,z)$ and
116 symbolize the BGS and SBS phase response at the location z from the pump launching end,
117 respectively. In the script, g_{SBS} is symbolized by the variables *SBS_g_log* and *SBS_gl_log* for the
118 conventional and engineered BGS in logarithm scale, respectively. P_p = 20 dBm (*P_pump* in the
119 script) is the pump pulse peak power at the fiber launching end; v_B is the BFS (normalized in the
120 script); g_0 = 0.2 W^{-1}m^{-1} (*g0* in the script) is the Brillouin gain coefficient; Δv_B = 50 MHz (*gamma_B*
121 in the script) is the FWHM of the BGS; α = 0.2 dB/km is the fiber loss coefficient and is represented
122 by *alpha_log* and *alpha_lin* as the value in logarithmic and linear scale in the script, respectively;
123 v is the probe wave frequency so that the pump and probe frequency offset $v - v_B$ is scanned from
124 -250 MHz to 250 MHz. The pump and probe frequency offset is represented in the script as the
125 global vector f. The term $g_1 = mg_0$ is the loss factor; $2d \cdot \Delta v_B$ is the frequency offset between the
126 two losses; and L_{eff} = 10 m (*L_eff* in the script) is the Brillouin interaction length for 100 ns pulse
127 width. The engineered spectral shape can be easily adjusted by tuning two normalized factors, m
128 and d. The conventional BGS can be modelled simply by $m = 0$.

129

130 1.2. Add random noise (i.e., additive white Gaussian noise) with the same level both on the

131 conventional and engineered BGS. Adjusting the parameter *noise_level* in the script can change
132 the noise level.

134 1.3. Fit the conventional noisy BGS with the Lorentzian function (*Lorentz_g_gain_fun* function in
135 the script) and the engineered noisy BGS with the superimposed Lorentzian function
136 (*Lorentz_gl_gain_fun* function in the script) (see **Figure 2A**).

138 1.4. Determine the peak frequency offset due to the noise for the conventional and engineered
139 BGS (**Figure 2B**).

141 1.5. Repeat steps 1.2–1.4 for $N = 500$ and collect all the peak frequency offsets Δf_{ci} and Δf_{pi}
142 (represented by *delta_g_g* and *delta_g_gl* in the script, respectively) for the conventional and
143 engineered BGS in the ith process, respectively.

145 [Place **Figure 2** here]

147 1.6. Calculate the ratio of the standard deviation of the noise-induced BFS estimation errors as:

149
$$\eta(m, d) = \sqrt{\frac{\frac{1}{N}\sum_1^N \Delta f_{pi}^2}{\frac{1}{N}\sum_1^N \Delta f_{ci}^2}} \tag{3}$$

151 1.7. Plot η as a function of m and d (see **Figure 3A**). Find the minimum value η_{min} and the
152 corresponding m and d. The advantage of the estimation accuracy will be maintained along the
153 whole fiber[28].

155 1.8. Tune the value of z (i.e., the fiber length, also z in the script) in Equation (2) from 0 km to 60
156 km, step 50 m and repeat steps 1.1–1.7 with some selected m and d values. Then the ratio of the
157 standard deviation as a function of the fiber length can be acquired (see **Figure 3B**).

159 **2. Prepare and test the conventional BOTDA setup (highlighted block in Figure 4B)**

161 2.1. Turn the laser diode (LD) on and check the functionality of the LD with the optical spectrum
162 analyzer (OSA). Usually, a wavelength around 1,550 nm is used.

164 2.2. Connect the LD with the 10:90 optical coupler (OC). Check the power from the 10% OC
165 output. If the power is higher than 13 dBm (the maximum input power of the polarization
166 scrambler [Pol.S.]), lower the LD output power by lowering the LD current.

168 2.3. Connect the 10% OC output with the Pol.S. In order to avoid polarization fading[1], set the
169 scrambling frequency to 1 kHz.

171 2.4. Check the power from the output of the Pol.S. If the power is higher than -3 dBm (the
172 maximum input power limit of the semiconductor optical amplifier [SOA]), add attenuators until

173   the power requirement is satisfied. Connect the Pol.S. with the SOA.

174

175   2.5. Apply the electrical pulse train signal with 100 ns pulse width and 4 kHz repetition rate from
176   the pulse generator (PG) on the SOA. Ensure that the amplitude of the pulse signal is higher than
177   the transistor-transistor logic (TTL) threshold of the SOA (i.e., 4 dBm) and the repetition rate
178   satisfies the round-trip requirement[30].

179

180   2.6. Connect the output from the SOA with the Erbium-doped fiber amplifier (EDFA 1) and
181   operate the EDFA in automatic current control (ACC) mode. Connect the output from EDFA 1 to
182   port 1 of the circulator (Cir).

183

184   2.7. Check the optical pulse signal from port 2 of Cir in the digitizer by connecting it with the
185   photodiode (PD). In order to avoid any damage to the PD, sufficient attenuation is necessary.

186

187   2.8. Calculate the optical pulse peak power by the waveform measured in the digitizer. The
188   optical peak power P_o is estimated according to

189

190     $$P_o = \frac{V_E}{RR_f} \tag{4}$$

191

192   where V_E is the electrical pulse peak voltage, and R and R_f are the PD responsivity and
193   transresistance. Take the protection attenuation into account in this calculation so that a correct
194   input pump power into the fiber under test (FUT, 10.6 km) is evaluated.

195

196   2.9. Note the EDFA current value I_{20} when the calculated optical pulse peak power reaches 20
197   dBm (MI threshold[19]). The extinction ratio (ER) of the optical pulse train can be evaluated
198   according to the conservation of energy:

199

200     $$P_{avg} \cdot \frac{1}{f_{rep}} = \frac{P_o}{ER} \cdot \frac{1}{f_{rep}} + P_o \cdot \tau \tag{5}$$

201

202   where P_{avg} is the optical average power of the pulse train; f_{rep} is the repetition rate; and τ is the
203   pulse width. The ER of the SOA is usually more than 30 dBm, efficiently avoiding NLE[31,32].

204

205   NOTE: Switch off the EDFA before disconnecting the PD and continuing to build the system.

206

207   2.10. Connect port 2 of the Cir with one end of the FUT to complete setting up the pump branch.
208   Check if the system will suffer from MI by checking the spectrum from the other end of the FUT
209   in the OSA and setting the EDFA at a constant current value, I_{20}. If the detected spectrum is the
210   same (in shape, not necessarily in amplitude) to the one measured in step 2.1, then the system
211   is free from MI. Otherwise, when obvious spectrum broadening or peak splitting[33] are observed,
212   reduce the EDFA 1 current to maintain the spectrum shape.

213

214   2.11. Connect the 90% output of the OC to a 50:50 OC 1 and connect one of the OC 1 outputs to
215   the Mach-Zehnder modulator (MZM 1) via a polarization controller (PC). Set the polarization

correctly, so that the output from MZM 1 is maximized (polarization alignment).

2.12. Apply the radio frequency (RF) signal from the RF generator (RFG 1) with the BFS of the FUT (for SSMF around 11 GHz) and 16 dBm amplitude to the MZM 1. Set the DC bias voltage of the MZM 1 so that the carrier is suppressed to the minimum.

2.13. Connect the output of the MZM 1 with fiber Bragg grating (FBG 1). Check the output spectrum from FBG 1 in the OSA so that the FBG 1 is set to block the upper frequency sideband and the carrier.

2.14. Connect the output from the FBG 1 to the EDFA 2, another 50:50 OC 2, and an isolator (ISO) consecutively.

2.15. Operate EDFA 2 also in ACC mode and set the current value to I_g, so that the output power from the ISO is lower than -14 dBm, minimizing NLE[20]. Switch off the EDFA before disconnecting the power meter and continue the system building. Connect the ISO output to the other end of the FUT to complete the setup building of the gain probe branch.

2.16. Connect the Cir port 3 to the EDFA 4 (for pre-amplification[34]) and PD. Set the EDFA to ACC mode. The current value I_4 should let the output power from EDFA be 4 smaller than the input limit of the PD. Connect the PD RF output to a 10 MHz RF low pass filter[35,36]. Connect the filter output to the digitizer.

2.17. Connect the trigger of the digitizer with the synchronized (or inverse) output of the pulse generator. Set the digitizer parameters as follows: Sampling rate: 500 MSa/s; averaging: 4,096 times; number of samples: 10,000.

2.18. Set the current value of EDFA 1, EDFA 2, and EDFA 4 to I_{20}, I_g, and I_4, respectively. Run a trace recording program. Check the trace measured in the digitizer. If the trace amplitude follows the intrinsic fiber loss decay, then the sensing system is MI free. Otherwise, reduce the current value of EDFA 1.

3. Measurement using the conventional BOTDA setup and data processing

3.1. Set the values of EDFA 1 and EDFA 2 to I_{20} and I_g, respectively. Scan the frequency of RFG 1 in the range of BFS ± 90 MHz with 1 MHz steps. Record the trace from the recording program after each scanning step.

3.2. Calculate the local Brillouin gain by dividing the trace amplitude (in Brillouin interaction period) by each DC offset (non-Brillouin interaction period).

3.3. Retrieve the BGS at each fiber section by fitting the measured noisy BGS with the Lorentzian fitting. Determine the FWHM of the conventional BGS Δv_{B0} from the fitting.

260 3.4. Repeat steps 3.1 and 3.2 for N = 48 times and collect all the estimated peak (BFS) frequency
261 distributions along the fiber $v_{Bci}(z)$ in the ith process (see **Figure 5A**).

263 3.5. Calculate the BFS estimation error as the standard deviation of the fitted BFS at each fiber
264 section in the 48 measurements (see **Figure 5B**).

266 **4. Preparing the rest of the setup**

268 NOTE: In this case, m = 1 and d = 1.24 were used, per simulation results (see section 1 and **Figure**
269 **3**).

271 4.1. Connect the other output of the 50:50 OC 1 in the probe branch with the EDFA 3 and the
272 50:50 OC 3.

274 4.2. Connect one of the outputs of 50:50 OC 3 to a PC and MZM 2. Adjust the polarization so that
275 the output from MZM 2 is maximized.

277 4.3. Apply the RF signal from RFG 2 with $BFS - d \cdot \Delta v_{B0}$ and 16 dBm amplitude on MZM 2. Check
278 the modulation spectrum in the OSA and adjust the bias voltage to minimize the carrier
279 amplitude.

281 4.4. Connect the output from MZM 2 to the input of an optical switch (OS 1), one of the inputs
282 of 50:50 OC 4, and the FBG 2.

284 4.5. Check the optical signal in the OSA and adjust the FBG 2 center wavelength so that the carrier
285 and the lower frequency sideband are blocked (see **Figure 4A**). The setup of the loss 1 probe
286 branch will then be complete.

288 4.6. Connect the other output of the 50:50 OC 3 to a PC and MZM 3. Adjust the polarization so
289 that the output from MZM 3 is maximized.

291 4.7. Apply the RF signal from the RFG 3 with $BFS + d \cdot \Delta v_{B0}$ and 16 dBm amplitude on MZM 3. Check
292 the modulation spectrum in the OSA and adjust the bias voltage to minimize the carrier
293 amplitude.

295 4.8. Connect the output from MZM 3 to a variable optical attenuator (VOA) with a switch function
296 (OS 2) and the other input of 50:50 OC 4. Considering that the offset between the loss probe
297 frequencies are relatively small in comparison to the FBG 2 transmission window (several GHz),
298 the carrier and the lower frequency sideband from MZM 3 will also be blocked by FBG 2. The
299 setup of the loss 2 probe branch will then be complete.

301 4.9. Close the OS 1, open the OS 2, and set the EDFA 3 current value to I_l so that the power of the
302 loss 1 probe equals -14 dBm (m = 1).

4.10. Open the OS 1, close the OS 2, and adjust the attenuation of VOA so that the power of the
305 loss 2 probe also equals -14 dBm.
306
307 **5. Measurement using the complete proposed BOTDA setup and data processing**
308
309 5.1. Close the OS 1, close the OS 2, and set the current value of EDFA 1, EDFA 2, EDFA 3, and EDFA
310 4 to I_{20}, I_g, I_l, and I_4, respectively. Scan the frequency of the RFG 1 in the range of BFS ± 90 MHz in
311 1 MHz steps. Frequencies from RFG 2 and RFG 3 scan correspondingly. Record the trace from the
312 program after each scanning step.
313
314 5.2. Calculate the local Brillouin gain as in step 3.2 and retrieve the engineered BGS at each fiber
315 section by fitting the measured noisy BGS with the superimposed Lorentzian function.
316
317 5.3. Repeat steps 5.1 and 5.2 for $N = 48$ times and collect all the estimated peak (BFS) frequency
318 distributions along the fiber $v_{Bpi}(z)$ in the ith process (see **Figure 5A**).
319
320 5.4. Calculate the BFS estimation error as the standard deviation of the fitted BFS at each fiber
321 section in the 48 measurements (see **Figure 5B**).
322
323 **REPRESENTATIVE RESULTS:**
324 **Figure 3** shows the simulation results. Points with $\eta < 1$ in **Figure 3A** indicate a smaller frequency
325 error (higher measurand resolution) with the engineered BGS. The lower the value was, the
326 bigger the advantage. The minimum ratio was at $m = 1$, indicating that a multiprobe instead of
327 multipump scheme can be carried out (see Discussion). **Figure 3B** shows the distribution of the
328 frequency error ratio η along the fiber with the selected parameters for m and d. The dash line
329 indicates the sensing range extension under the same frequency error tolerance (measurand
330 resolution requirement). The maximum sensing range extension of 60% is shown. The
331 experiment was conducted with the setup scheme illustrated in **Figure 4B**. **Figure 6A** shows the
332 typical conventional and proposed BGS with their corresponding fittings. The time domain traces
333 of the selected points on the spectrum are depicted in **Figure 6B**. The BFS in both methods were
334 determined from the peak frequencies of the fittings. The BFS distribution along the fiber
335 examined by both methods is plotted in **Figure 5A**. After 48 measurements, the standard
336 deviations of the 48 determined the BFS at each fiber section were calculated and plotted in
337 **Figure 5B**. Due to the exponential decreasing SNR, the frequency errors also follow an
338 exponential increase.
339
340 **FIGURE LEGENDS:**
341 **Figure 1: Schematic of an engineered BGS by the superposition of one Brillouin gain and two**
342 **symmetric Brillouin loss spectra.**
343
344 **Figure 2: Simulated BGS.** (**A**) Demonstration of the fitting of a typical Lorentzian (red) and
345 engineered (blue) BGS in the simulation. (**B**) The Lorentzian BGS peak from (**A**). Δf_{ci} represents
346 the BFS estimation error for the conventional BGS in the ith measurement.
347

348 **Figure 3: Simulation results.** (**A**) The frequency error ratio as a function of m and d in the
349 simulation after 500 calculations. The minimum ratio of 47% was achieved with $m = 1$ and $d =$
350 1.24 (highlighted point). (**B**) The distribution of the frequency error ratio along the fiber with
351 selected m and d values. The dashed lines indicate the sensing range extension under the same
352 frequency error tolerance.

354 **Figure 4: Experimental setup scheme.** (**A**) The experimental multiprobe scheme and (**B**) the setup
355 in detail. The highlighted part of the setup denotes a conventional BOTDA system. LD: laser diode,
356 OC: optical coupler, Pol.S.: polarization scrambler, PG: pulse generator, SOA: semiconductor
357 optical amplifier, EDFA: Erbium-doped fiber amplifier, Cir: circulator, RFG: radio frequency
358 generator, MZM: Mach-Zehnder modulator, FBG: fiber Bragg grating, ISO: isolator, OS: optical
359 switch, VOA: variable optical attenuator, PD: photodiode, FUT: fiber under test.

361 **Figure 5: Experimental results.** (**A**) BFS distribution along the fiber with the conventional (black)
362 and engineered (red) BGS[28]. The estimated BFS with the engineered BGS showed the same but
363 clearer distribution along the fiber compared to the conventional BGS, which indicated the better
364 functionality of the proposed sensor. (**B**) The frequency error distribution along the fiber with
365 conventional (black) and engineered (red) BGS and their corresponding exponential fittings
366 (highlighted)[28]. The standard deviation verified that the frequency error was reduced by a factor
367 of two. Thus, under the same frequency error tolerance, the sensing range could be drastically
368 extended.

370 **Figure 6: Experimental results.** (**A**) The conventional (black) and engineered (red) BGS with their
371 corresponding fittings[28]. (**B**) The time domain traces at the maximum gain of the conventional
372 (black) and engineered BGS (blue), and at the maximum loss of the engineered BGS (orange),
373 corresponding to the points A, B, and C in the frequency domain labelled in (**A**), respectively. The
374 different noise amplitude between the traces indicated that the sensing system suffered not only
375 from the common-mode noise but was also significantly influenced by an active noise source
376 from the SBS interaction. This Brillouin intensity noise level was highly pump power dependent
377 (comparison between trace A and B) and can be avoided in Brillouin loss interactions (trace C).

379 **DISCUSSION:**
380 The most critical step during the experiment is the equalization of the three probe powers so
381 that $m = 1$ and symmetry between the two Brillouin loss spectra is achieved. Besides the separate
382 power check using the power meter at Cir port 2, as presented in steps 4.9 and 4.10, the power
383 equalization can be more precisely checked in the digitizer. By setting the RF 1 frequency to ~11
384 GHz (the fiber BFS) and switching off EDFA 3, the conventional trace with the peak gain can be
385 recorded in the digitizer (trace I). Then the RF 2 and RF 3 frequency are set to $BFS - d \cdot \Delta v_{B0}$ and
386 $BFS + d \cdot \Delta v_{B0}$, respectively. By switching EDFA 2 off but EDFA 3 on, the trace with the maximum
387 loss in the lower (trace 2) and upper frequency (trace 3) are recorded by closing OS 1 and OS 2,
388 respectively. When all three traces have the same amplitude as the DC offset (SBS gain is equal
389 to the loss), the three probe powers are well equalized. Fine tuning the current value of EDFA 2,
390 EDFA 3, and the attenuation of VOA can adjust the amplitude of the three traces individually.

The implementation of the RF filter before the PD not only reduces the common-mode noise level[35,36], but also avoids four wave mixing (FWM) and interference between the loss probe waves. Therefore, the optimal filter bandwidth is not only pump pulse width dependent[35], but also dependent on the parameter d. A suitable RF filter should effectively block the beating frequency components between the loss probe waves, which would be in the range of several hundred MHz. This can be checked by the RF spectrum in an electrical spectrum analyzer after the PD, when both loss probe waves are launched into the fiber.

The implementation of the multiprobe scheme restricts the constant m to $m = 1$. However, this is not a disadvantage, because according to the simulation results, the best performance will be achieved with $m = 1$. Also, the multiprobe scheme not only simplifies the experimental setup, but also circumvents FWM caused by the copropagation of multipulses.

The significance of the protocol is the enhancement of the SNR in an unprecedented, novel way. The well-engineered spectrum sharpens the peak and reduces the ambiguity against the system noise. Though this paper only demonstrates an instance where 100 ns pulses (10 m spatial resolution) are applied, this method is still valid when the pulse width is shortened and the FWHM of the generated conventional BGS is broadened due to the finite phonon lifetime. The only difference is that the optimal m and d values may vary. Theoretically, a BGS in a delta-function profile will remove all the ambiguity. However, it is hard to achieve this limit due to the finite lifetime of the acoustic wave. This work will inspire new investigations on further optimization of the gain spectrum with a higher contrast. Sensors using the proposed technique will be very valuable to sensing tasks requiring long sensing ranges or high measurement accuracy.

REFERENCES:
1. Motil, A., Bergman, A., Tur, M. [INVITED] State of the art of Brillouin fiber-optic distributed sensing. *Optics & Laser Technology*. **78**, 81–103 (2016).
2. Kurashima, T., Tateda, M. Thermal effects on the Brillouin frequency shift in jacketed optical silica fibers. *Applied Optics*. **29** (15), 2219–2222 (1990).
3. Horiguchi, T., Kurashima, T., Tateda, M. Tensile strain dependence of Brillouin frequency shift in silica optical fibers. *IEEE Photonics Technology Letters*. **1** (5), 107–108 (1989).
4. Preussler, S., Wiatrek, A., Jamshidi, K., Schneider, T. Brillouin scattering gain bandwidth reduction down to 3.4MHz. *Optics Express*. **19** (9), 8565–8570 (2011).
5. Wiatrek, A., Preußler, S., Jamshidi, K., Schneider, T. Frequency domain aperture for the

436   gain bandwidth reduction of stimulated Brillouin scattering. *Optics Letters*. **37** (5), 930–
437   932 (2012).

438 6.   Preussler, S., Schneider, T. Bandwidth reduction in a multistage Brillouin system. *Optics*
439   *Letters*. **37** (19), 4122–4124 (2012).

440 7.   Preussler, S., Schneider, T. Stimulated Brillouin scattering gain bandwidth reduction and
441   applications in microwave photonics and optical signal processing. *Optical Engineering*. **55**
442   (3), 031110 (2015).

443 8.   Wei, W., Yi, L., Jaouen, Y., Morvan, M., Hu, W. Brillouin Rectangular Optical Filter with
444   Improved Selectivity and Noise Performance. *IEEE Photonics Technology Letters*. **27** (15),
445   1593–1596 (2015).

446 9.   Feng, C., Preussler, S., Schneider, T. The Influence of Dispersion on Stimulated Brillouin
447   Scattering Based Microwave Photonic Notch Filters. *Journal of Lightwave Technology*. **36**
448   (22), 5145–5151 (2018).

449 10.   Feng, C., Preussler, S., Schneider, T. Investigation of the Dispersion Effect on Stimulated
450   Brillouin Scattering based Microwave Photonic Notch Filters. *2018 International Topical*
451   *Meeting on Microwave Photonics (MWP)*. 1–4 (2018).

452 11.   Feng, C., Preussler, S., Schneider, T. Sharp tunable and additional noise-free optical filter
453   based on Brillouin losses. *Photonics Research*. **6** (2), 132–137 (2018).

454 12.   Henker, R. et al. Gain enhancement in multiple-pump-line Brillouin-based slow light
455   systems by using fiber segments and filter stages. *Applied Optics*. **48** (29), 5583–5588
456   (2009).

457 13.   Zhang, L. et al. Superluminal propagation at negative group velocity in optical fibers based
458   on Brillouin lasing oscillation. *Physical Review Letters*. **107** (9), 93903 (2011).

459 14.   Xing, L., Zhan, L., Xia, Y. Large delay tunable slow-light based on high-gain stimulated-
460   Brillouin-scattering amplification in optical fibers. *Chinese Science Bulletin*. **54** (21), 3947–
461   3952 (2009).

462 15.   Preussler, S., Wiatrek, A., Jamshidi, K., Schneider, T. Ultrahigh-resolution spectroscopy
463   based on the bandwidth reduction of stimulated brillouin scattering. *IEEE Photonics*
464   *Technology Letters*. **23** (16), 1118–1120 (2011).

465 16.   Horiguchi, T., Tateda, M. Optical-fiber-attenuation investigation using stimulated Brillouin
466   scattering between a pulse and a continuous wave. *Optics Letters*. **14** (8), 408–410 (1989).

467 17.   Feng, C., Emad Kadum, J., Schneider, T. The State-of-the-Art of Brillouin Distributed Fiber
468   Sensing. *Brillouin Distributed and Fiber-bragg-grating-based Fiber Sensing - Principle,*
469   *Measurement and Applications*. (2019).

470 18.   Soto, M. A., Thévenaz, L. Modeling and evaluating the performance of Brillouin distributed
471   optical fiber sensors. *Optics Express*. **21** (25), 31347–66 (2013).

472 19.   Alem, M., Soto, M. A., Thévenaz, L. Analytical model and experimental verification of the
473   critical power for modulation instability in optical fibers. *Optics Express*. **23** (23), 29514–
474   29532 (2015).

475 20.   Thévenaz, L., Mafang, S. F., Lin, J. Effect of pulse depletion in a Brillouin optical time-
476   domain analysis system. *Optics Express*. **21** (12), 14017–14035 (2013).

477 21.   Iribas, H., Urricelqui, J., Mompó, J. J., Mariñelarena, J., Loayssa, A. Non-Local Effects in
478   Brillouin Optical Time-Domain Analysis Sensors. *Applied Sciences*. **7** (8), 761 (2017).

479 22.   Soto, M. A., Le Floch, S., Thévenaz, L. Bipolar optical pulse coding for performance

480   enhancement in BOTDA sensors. *Optics Express*. **21** (14), 16390–16397 (2013).

481 23. Angulo-Vinuesa, X., Martin-Lopez, S., Corredera, P., Gonzalez-Herraez, M. Raman-assisted
482   Brillouin optical time-domain analysis with sub-meter resolution over 100 km. *Optics*
483   *Express*. **20** (11), 12147 (2012).

484 24. Haneef, S. M., Yang, Z., Thévenaz, L., Venkitesh, D., Srinivasan, B. Performance analysis of
485   frequency shift estimation techniques in Brillouin distributed fiber sensors. *Optics Express*.
486   **26** (11), 14661–14677 (2018).

487 25. Lopez-Gil, A. et al. Evaluation of the accuracy of BOTDA systems based on the phase
488   spectral response. *Optics Express*. **24** (15), 17200–17214 (2016).

489 26. Urricelqui, J., Soto, M. A., Thévenaz, L. Sources of noise in Brillouin optical time-domain
490   analyzers. *24th International Conference on Optical Fibre Sensors*. **9634**, 963434 (2015).

491 27. Zornoza, A., Sagues, M., Loayssa, A. Self-heterodyne detection for SNR improvement and
492   distributed phase-shift measurements in BOTDA. *Journal of Lightwave Technology*. **30** (8),
493   1066–1072 (2012).

494 28. Feng, C., Lu, X., Preussler, S., Schneider, T. Gain Spectrum Engineering in Distributed
495   Brillouin Fiber Sensors. *Journal of Lightwave Technology*. **37** (20), 5231–5237 (2019).

496 29. Feng, C., Lu, X., Preussler, S., Schneider, T. Measurement accuracy enhancement of
497   distributed Brillouin sensors based on gain spectrum engineering. *Seventh European*
498   *Workshop on Optical Fibre Sensors*. **11199**, 9 (2019).

499 30. Peled, Y., Motil, A., Tur, M. Fast Brillouin optical time domain analysis for dynamic sensing.
500   *Optics Express*. **20** (8), 8584–8591 (2012).

501 31. Feng, C., Iribas, H., Marinelaerña, J., Schneider, T., Loayssa, A. Detrimental Effects in
502   Brillouin Distributed Sensors Caused By EDFA Transient. *Conference on Lasers and Electro-*
503   *Optics*. JTu5A.85 (2017).

504 32. Iribas, H. et al. Effects of pump pulse extinction ratio in Brillouin optical time-domain
505   analysis sensors. *Optics Express*. **25** (22), 27896–27911 (2017).

506 33. Tai, K., Hasegawa, A., Tomita, A. Observation of modulational instability in optical fibers.
507   *Physical Review Letters*. **56** (2), 135–138 (1986).

508 34. De Souza, K., Newson, T. P. Brillouin-based fiber-optic distributed temperature sensor with
509   optical preamplification. *Optics Letters*. **25** (18), 1331 (2000).

510 35. Feng, C., Preussler, S., Emad Kadum, J., Schneider, T. Measurement Accuracy Enhancement
511   via Radio Frequency Filtering in Distributed Brillouin Sensing. *Sensors*. **19** (13), 2878 (2019).

512 36. Kadum, J., Feng, C., Preussler, S., Schneider, T. Improvement of the measurement accuracy
513   of distributed Brillouin sensing via radio frequency filtering. *Seventh European Workshop*
514   *on Optical Fibre Sensors*. **19** (13), 3 (2019).
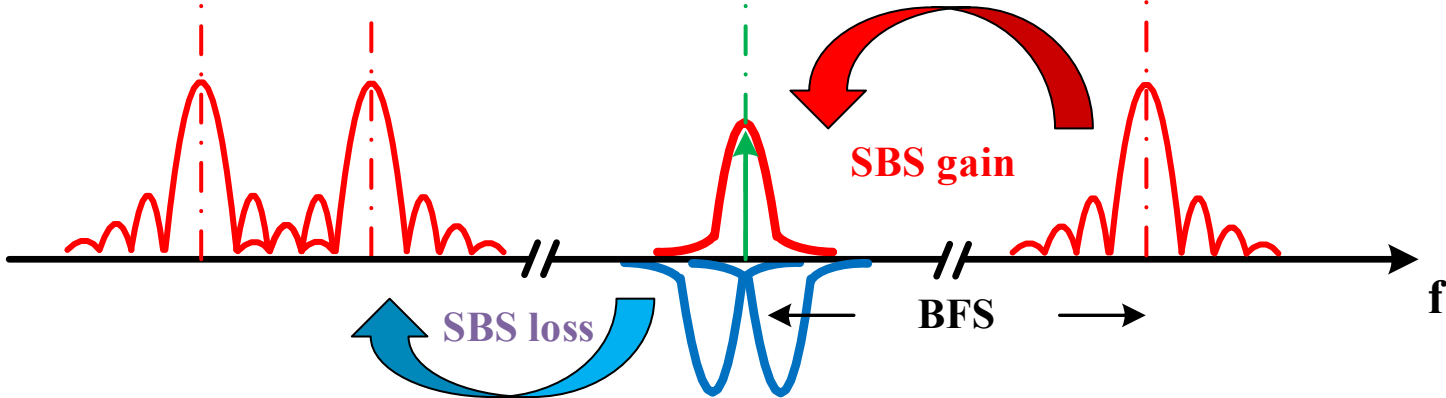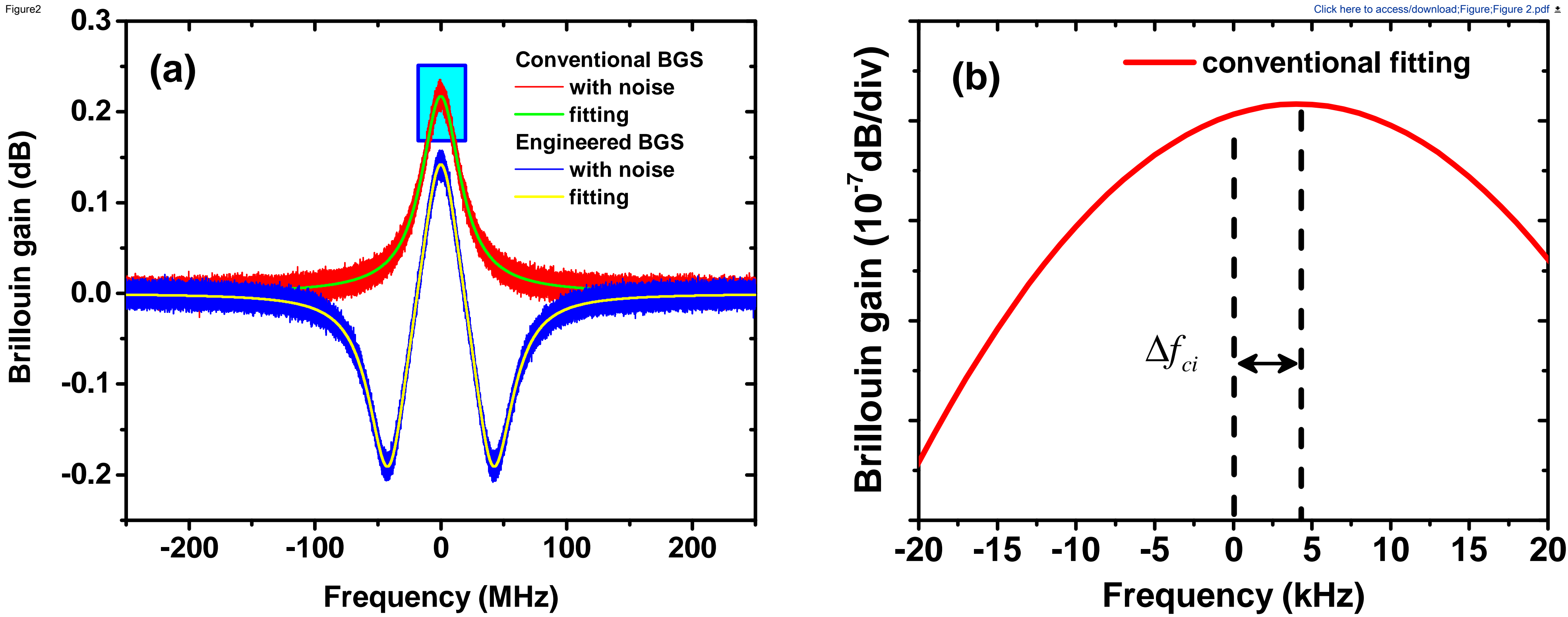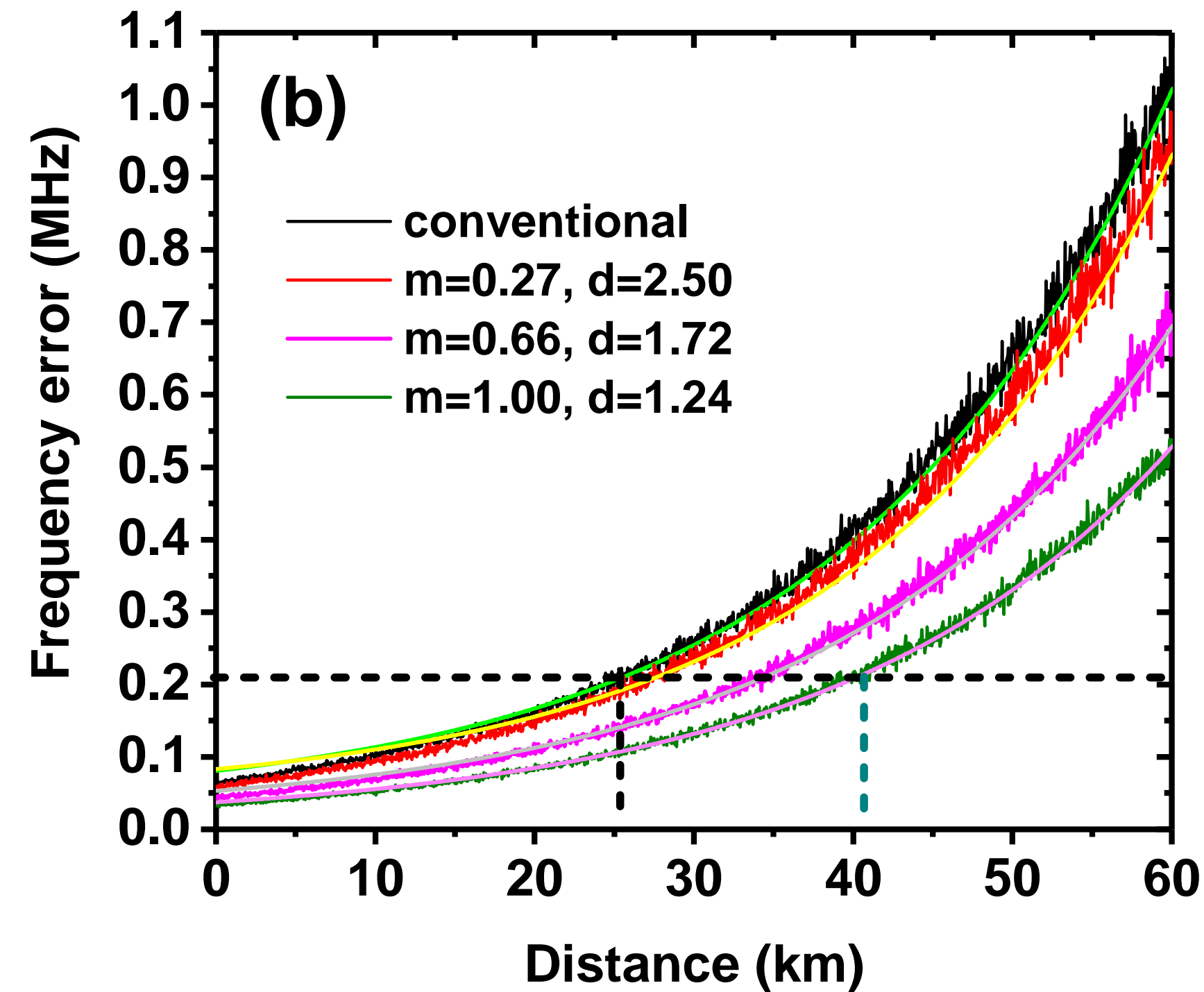
515

Loss pumps Probe Gain pump

SBS gain

SBS loss
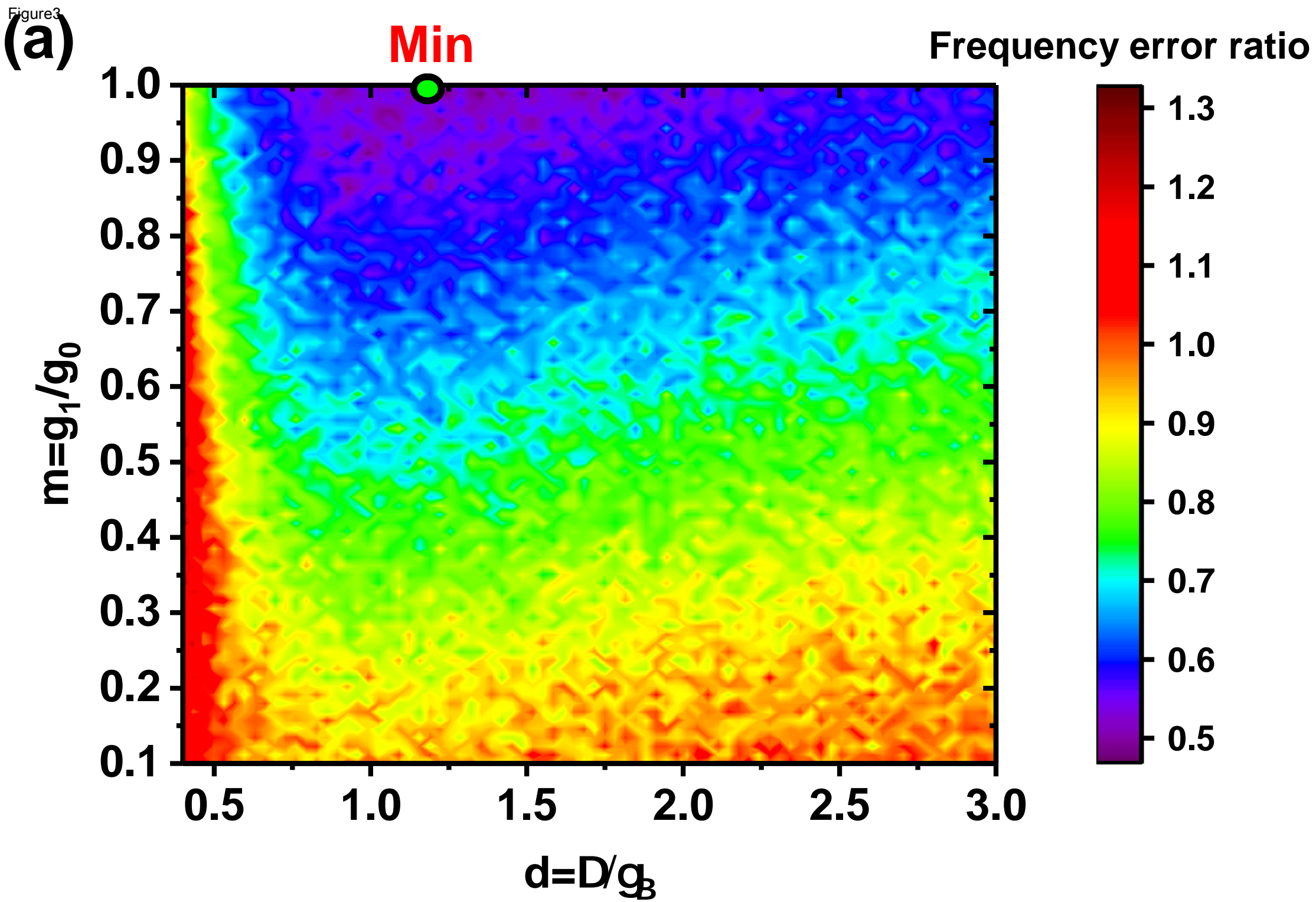
BFS

f
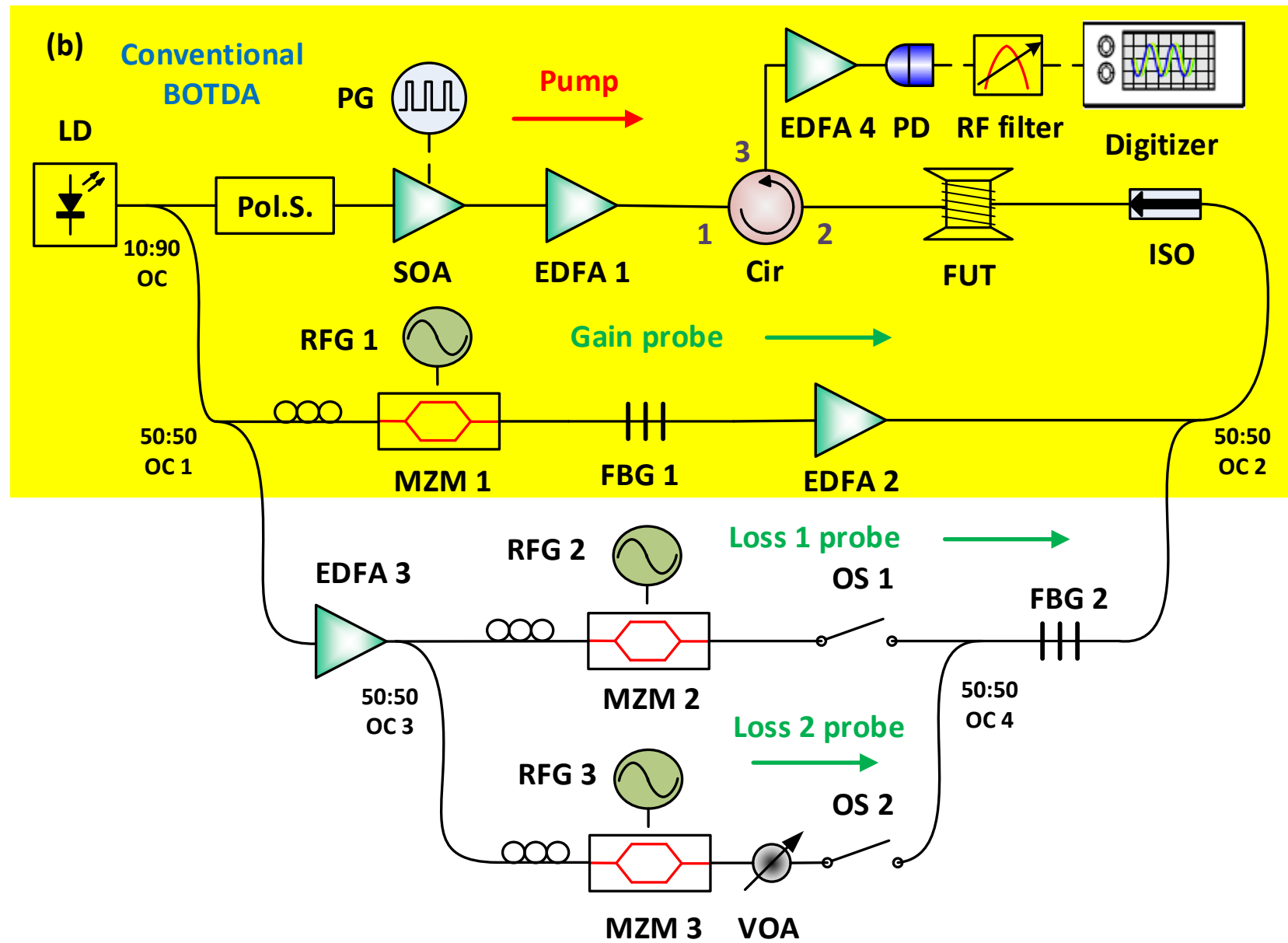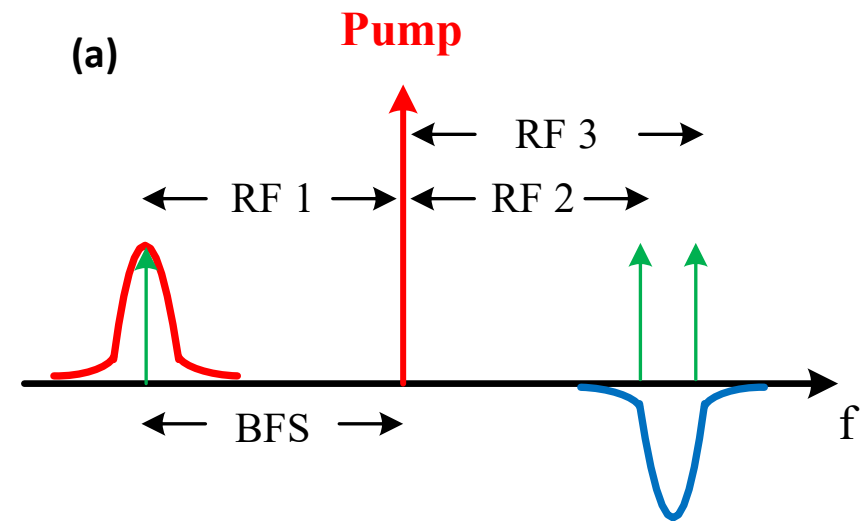
Figure2

Figure3

(a) Pump, RF 1, RF 2, RF 3, BFS, f

(b) Conventional BOTDA

LD, 10:90 OC, Pol.S., PG, SOA, Pump, EDFA 1, Cir, FUT, ISO, EDFA 4, PD, RF filter, Digitizer

RFG 1, Gain probe, 50:50 OC 1, MZM 1, FBG 1, EDFA 2, 50:50 OC 2

EDFA 3, RFG 2, Loss 1 probe, OS 1, MZM 2, FBG 2, 50:50 OC 3, 50:50 OC 4

RFG 3, Loss 2 probe, OS 2, MZM 3, VOA

Figure5

Figure6
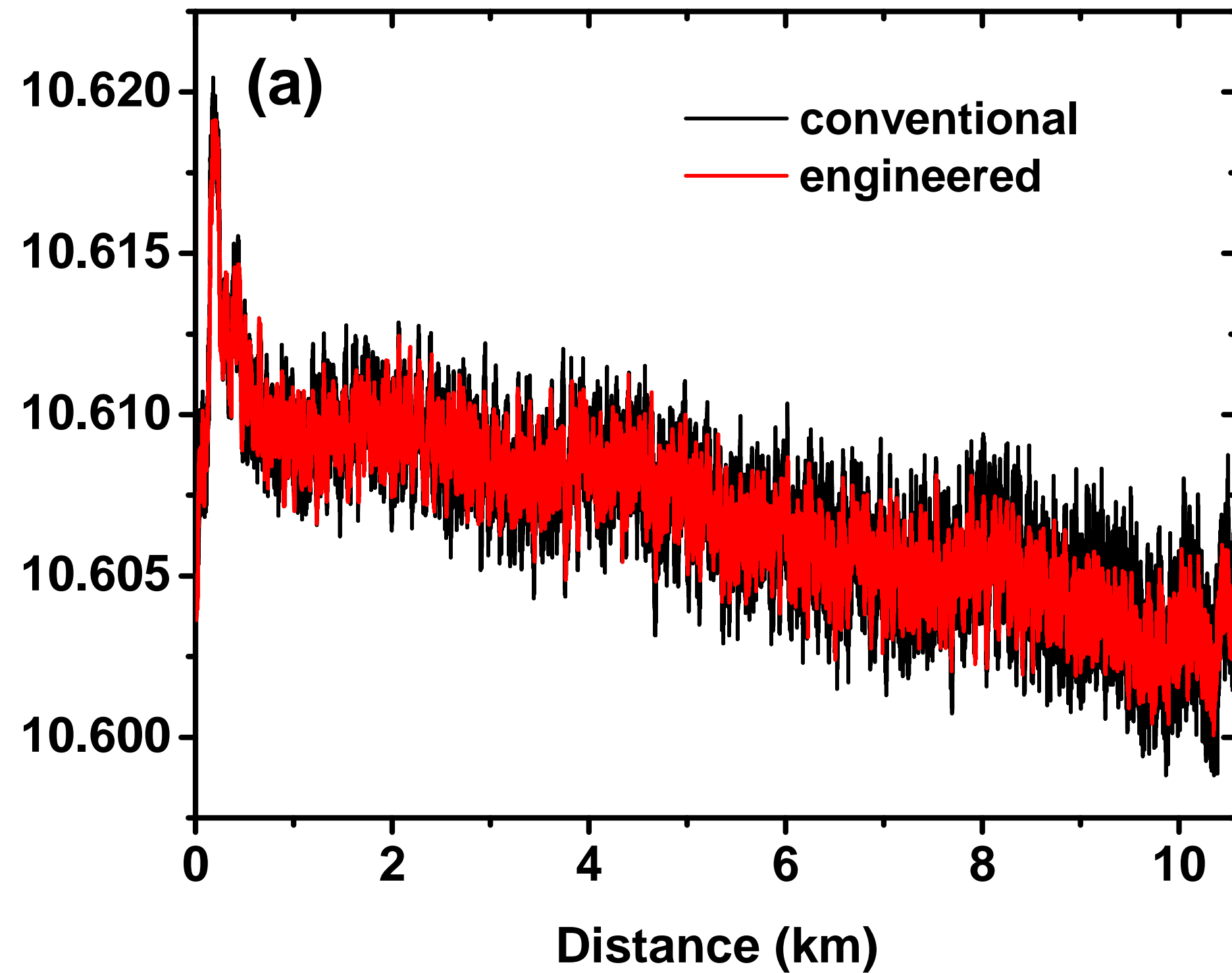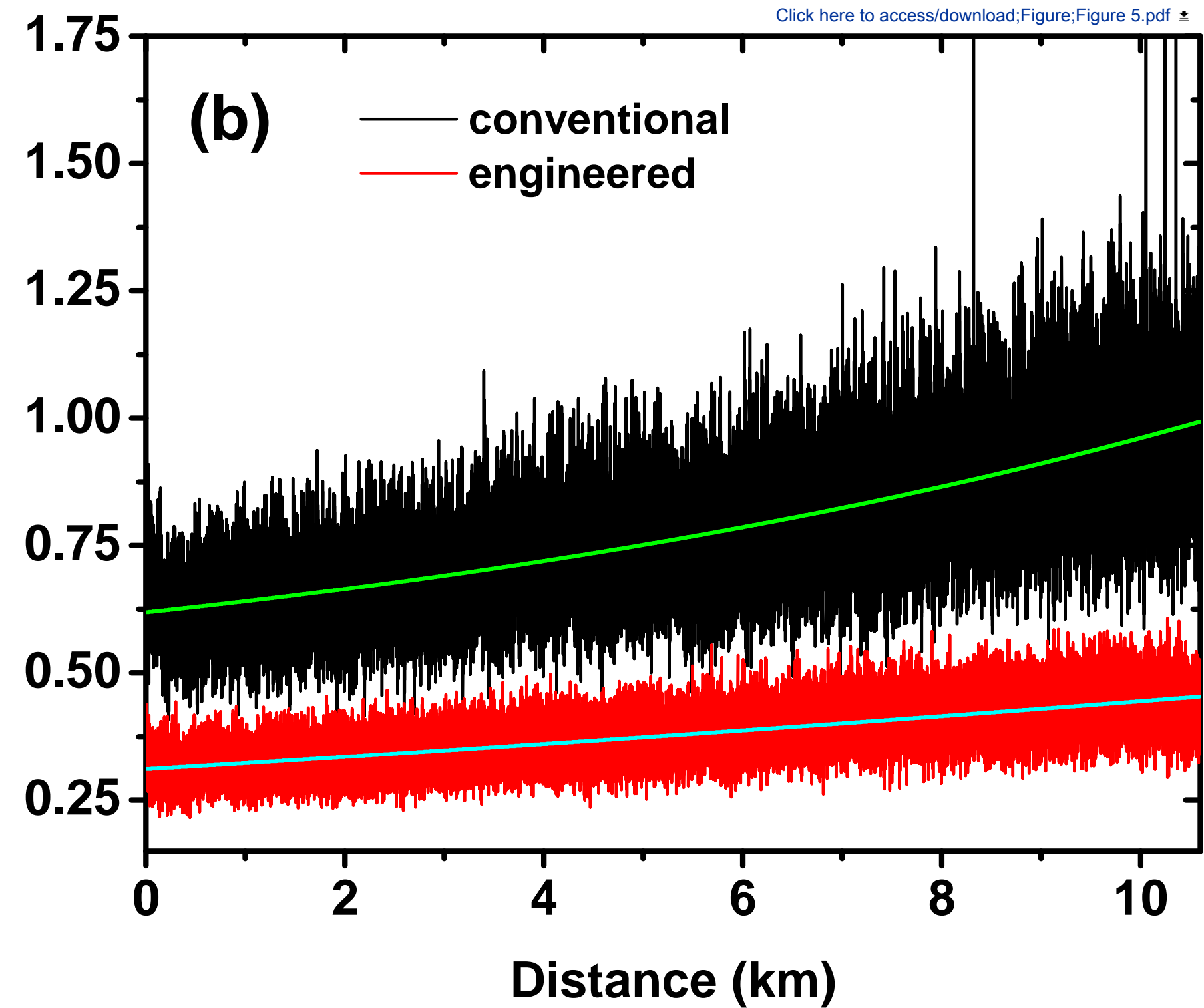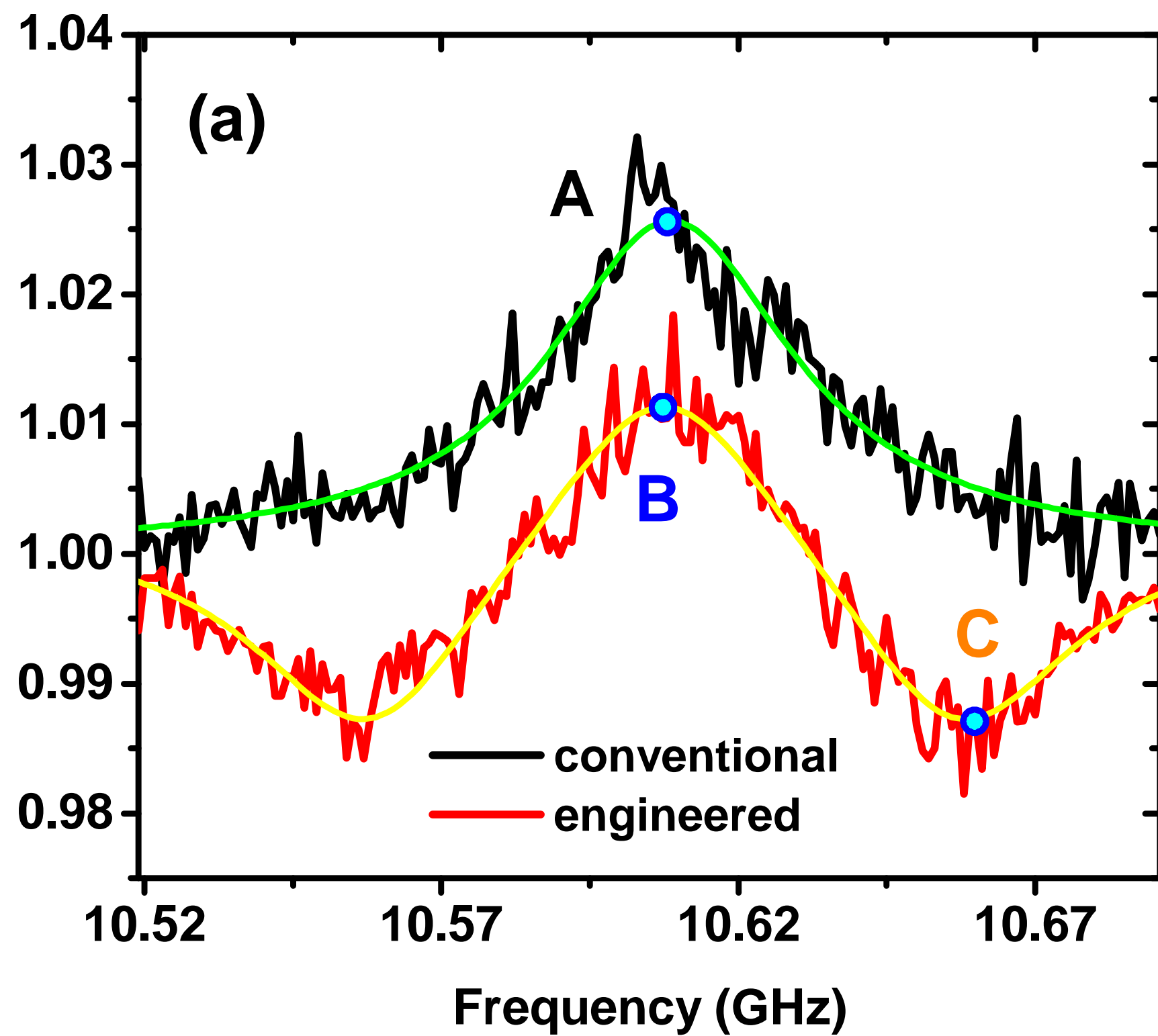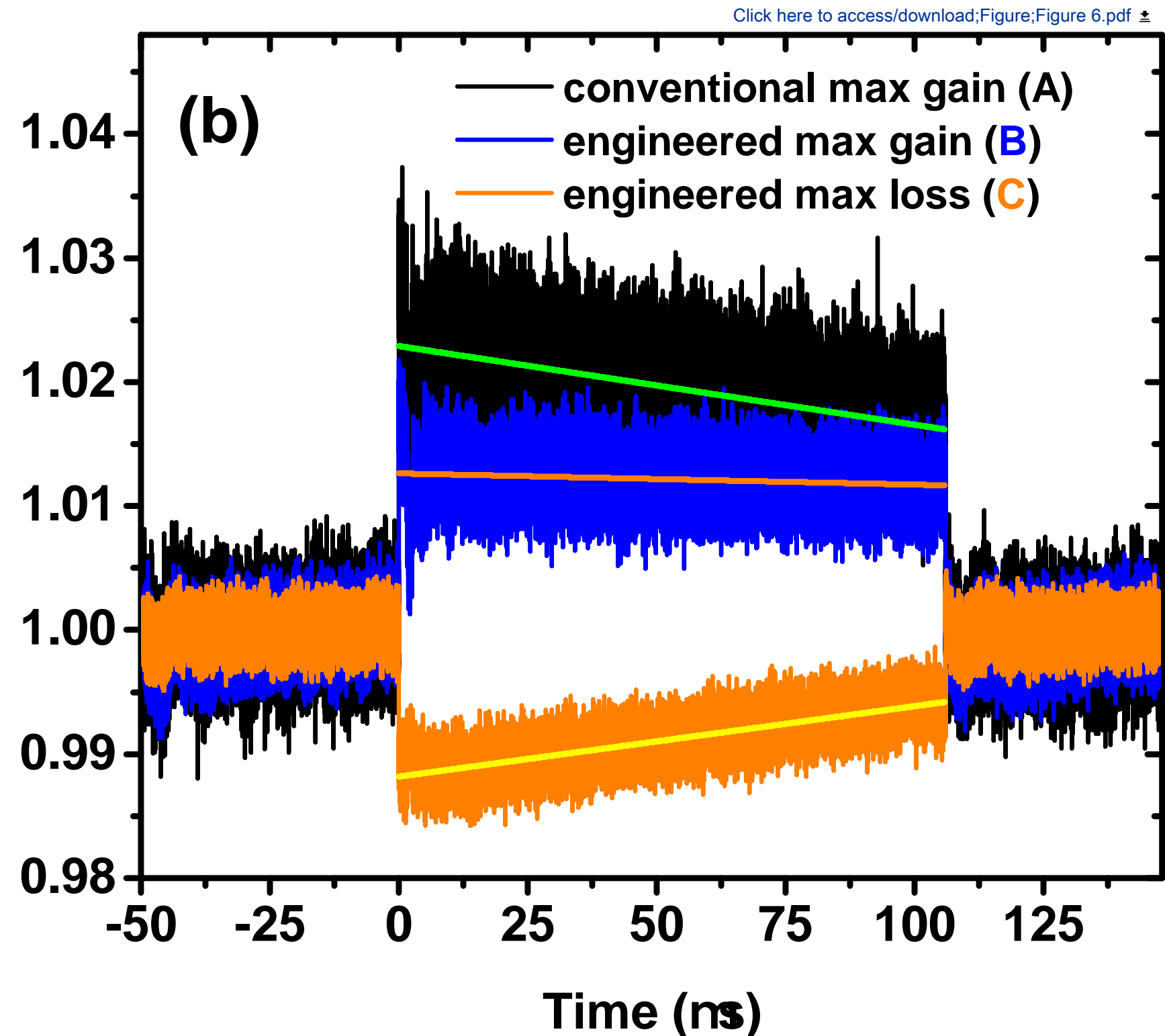
Table of Materials

Name of Material/Equipment	Company	Catalog Number
Current controller for laser diode	ILX Lightwave	LDX3220
Digitizer	Acqiris SA	U5309A-1039
Erbium doped fiber amplifier 1	Photop	PTEDFA-A-PA-C-SCH-15
Erbium doped fiber amplifier 2	LiComm	OFA-TCH
Erbium doped fiber amplifier 3	Calmar Optcom	AMP-ST30
Erbium doped fiber amplifier 4	Photop	PTEDFA-A-PA-C-SCH-15
Fiber Bragg grating 1	Advanced Optics Solutions	T-FBG
Fiber Bragg grating 2	Advanced Optics Solutions	T-FBG
Fiber under test	ofs	
Isolator	General Photonics	S-15-NTSS
Laser diode	3SP Group	A1905 LMI
Mach-Zehnder modulator 1	Avanex	IM10
Mach-Zehnder modulator 2	Avanex	IM10
Mach-Zehnder modulator 3	Avanex	IM10
Nanosecond driving board for semiconductor optical amplifier	Highland Technology	T160-9 (28A160-9C)
Optical coupler 10:90	Newport	
Optical coupler 50:50	Newport	
Optical spectrum analyzer	Hewlett Packard	86145A
Optical switch 1	JDSU	SN12-1075NC
Photodiode	Thorlabs	D400FC
Polarization scrambler	General Photonics	PSY-101
Pulase generator	Hewlett Packard	8082A
Radio function generator 1	Anritsu	MG3692C
Radio function generator 2	Agilent Technology	E8257D
Radio function generator 3	HTM	T2100
Semiconductor optical amplifier	Thorlabs	SOA1013SXS
Temperature controller for laser diode	ILX Lightwave	LDT5948
Temperature controller for semiconductor optical amplifier	Tektronix	TED200
Variable optical attenuator	JDSU	mVOA-A1

Comments/Description

Benchtop coupler/WDM
Benchtop coupler/WDM

With optical switch function

Dear editors,

This paper is the re-revision to manuscript JoVE61115. We would like to thank the editors for their careful reviews and invaluable comments.

We have revised the manuscript according to the comments and suggestions from the editors. The manuscript is revised with tracking mode. For your convenience, in this response letter we have included the editor's and reviewers' original comments in *italic*, with our answers in **bold**, and our revisions in the manuscript **bold** and **highlighted**.

----------*Editorial comments:*----------
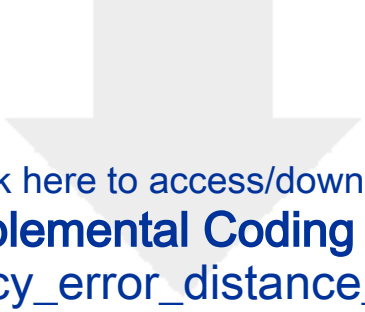
General:

1. *Please explain how to implement 1.2-1.8 in MATLAB. Including a complete supplementary script and explaining which parameters to change instead of embedding code may be best.*
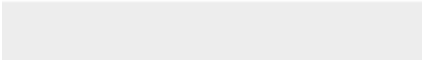
Thank you very much for the suggestion. The complete MATLAB script is supplemented in this submission via the submission system. Additional explanations have been added in steps 1.1)-1.8) with tracking mode.

2. *2.8, 2.9: Are the equations in these steps necessary to show in the video? It may be possible to include the equations themselves as overlaid text but not their explanations. Otherwise we could refer viewers to the text.*

Thank you very much for the suggestions. It is not necessary to show the equations in the video. Simply referring the viewers to the text for more details would be more appropriate. The highlighted parts have been cancelled in the corresponding context.
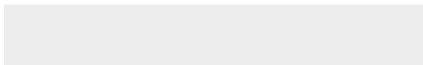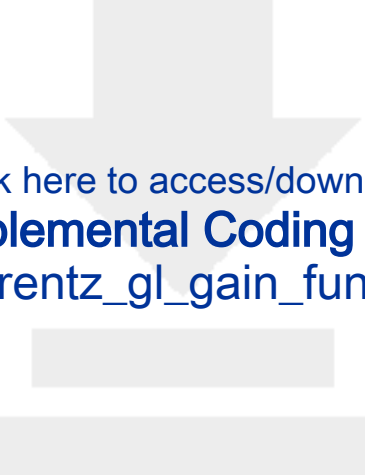
Click here to access/download

Supplemental Coding Files
Lorentz_g_gain_fun.m

Click here to access/download

Supplemental Coding Files
Lorentz_gl_gain_fun.m

Click here to access/download

Supplemental Coding Files

SBS_g.m

Click here to access/download
Supplemental Coding Files
SBS_gl.m